

PARTICLE IDENTIFICATION USING DE/DX
IN THE MARK II DETECTOR AT THE SLC*

A. BOYARSKI, D. P. COUPAL, G. J. FELDMAN, G. HANSON,
J. NASH, K. F. O'SHAUGHNESSY, P. RANKIN[†], R. VAN KOOTEN

*Stanford Linear Accelerator Center
Stanford University, Stanford, California 94309*

ABSTRACT

The central drift chamber in the Mark II detector at the SLAC Linear Collider has been instrumented with 100-MHz Flash-ADCs. Pulse digitization provides particle identification through the measurement of average ionization loss in the chamber. We present the results of a study of system performance and outline the systematic corrections that optimize resolution. The data used are from a short test run at PEP with one-third of the FADCs installed and an extensive cosmic ray sample with the fully instrumented chamber.

*Presented at the 5th International Wire Chamber Conference:
Recent Trends and Alternative Techniques, Vienna, Austria, February 13-17, 1989*

* Work supported by the Department of Energy, contract DE-AC03-76SF00515.

† Present Address: University of Colorado, Boulder, Colorado 80309

1. Introduction

The upgraded Mark II detector is the first experiment to look at e^+e^- collisions at the new SLAC Linear Collider (SLC). The wide range of physics that can be studied requires a general purpose detector with momentum analysis for charged tracks, electromagnetic calorimetry and particle identification. A time-of-flight system of scintillation counters is used for identification of low momentum particles and the calorimetry is used for high momentum electrons. To cover the intermediate range from approximately 400 MeV/c to 10 GeV/c, the new drift chamber has been instrumented with 100 MHz Flash-ADC (FADC) readout to provide particle identification through the measurement of average ionization loss.

This paper describes the work done in understanding and optimizing the particle identification performance of the FADC system. In the next section we give a brief description of the chamber and FADC system. The following sections describe the corrections used to optimize resolution, comparisons of data with models of ionization loss, and particle separation performance.

2. Drift Chamber Description

The drift chamber is described in detail elsewhere [1]. We give here a brief description of the chamber design and electronics.

2.1. CHAMBER DESIGN

The chamber is cylindrical with an inner radius of 0.19 m, an outer radius of 1.52 m, and an active length of 2.3 m. It consists of 12 concentric layers of cells with 6 sense wires per cell. This arrangement provides 72 measurements of track position and ionization for tracks traversing all layers ($|\cos\theta| < 0.6$, where θ is the angle between the track and the chamber axis). For tracks perpendicular to the sense wires, the ionization is collected over a gas length of 8.33 mm. There is a total of 972 cells, or 5832 sense wires. Odd-numbered layers are axial and

even-numbered layers are alternately $+3.8$ and -3.8 degrees stereo. The chamber operates in a solenoidal magnetic field of 4.75 kG and is filled with a gas mixture of 89% Argon, 10% CO_2 , and 1% methane at atmospheric pressure.

The cell design is shown in fig. 1. The six sense wires are staggered $\pm 380\mu\text{m}$ to resolve left-right ambiguity. The 19 field wire voltages are set so as to produce a uniform drift field. The guard wires provide additional field shaping and isolate the cell from the effects of neighboring cell layers. The potential wires control the sense wire gain and reduce the electrostatic deflection of the staggered sense wires. Typical operating voltages result in a gas gain of 2×10^4 and a drift field of 900 V/m. The magnetic field shifts the electron drift direction by 19 degrees away from perpendicular to the sense wire plane.

2.2. ELECTRONICS AND DATA ACQUISITION

The signals from the sense wires are amplified in preamplifiers mounted on the chamber face. This circuit contains coupling resistors that cancel crosstalk between nearest and next-to-nearest neighboring channels. The signal is then sent to postamplifier circuitry mounted on the outside of the detector that further amplifies and shapes the signal to remove the slow $1/t$ tail. A discriminated pulse is then sent to a TDC system and an amplified pulse is sent to the FADC system. Details of the preamplifier and postamplifier can be found in ref. [2].

The FADC design [3] is based on the 100-MHz 6-bit TRW 1029J7C FADC chip. With 16 channels per FASTBUS module, the entire system is contained in 18 FASTBUS crates. It runs on a single 100-MHz clock that synchronizes to a start signal. Zero suppression is achieved using circuitry within each module that finds leading and trailing edges in the data memory based on a threshold stored in the module. The thresholds are written into the module by the online computer.

The data are read out using a SLAC Scanner Processor (SSP) [4] located in each crate. Fig. 2 shows an example of the FADC data for two tracks crossing in a cell. The SSP applies a “difference of samples” (DOS) algorithm [5] to the digitized

pulse string to find improved leading and trailing edges for each hit and to separate overlapping pulses. The pedestal-subtracted area of the pulse is calculated and should be proportional to the charge deposited for that hit. A drift time for each pulse is determined by forming a weighted average over the time bins immediately following the leading edge found by the DOS algorithm. Using this drift time, programs on the online computer correlate TDC and FADC hits on each wire, and assign the measured ionization sample to a particular track. For testing FADC pulse algorithms, the raw digitized pulse can be saved on tape as well as the time and area. Currently, only complicated pulse shapes that may occur for closely-spaced tracks are saved for offline analysis. The DOS algorithm's ability to resolve closely-spaced hits is shown in fig. 3 compared to the separation using TDC hits alone.

3. Results

3.1. DATA SAMPLES

Two data samples have been used to study systematic corrections to the ionization loss. One-third of the chamber was instrumented with FADCs during a test run of the upgraded Mark II at PEP. At a center-of-mass energy of 29 GeV, the PEP data consists primarily of $e^+e^- \rightarrow$ hadrons (mostly π , K, and p) and Bhabha scattering events which produce back-to-back electron-positron pairs in the detector. Since the move to the SLC interaction region, the entire chamber has been instrumented and a large sample of cosmic rays has been collected to study various systematic corrections in detail.

3.2. SYSTEMATIC CORRECTIONS

Systematic errors have to be reduced as much as possible in order to approach the expected dE/dx resolution. Each ionization sample is corrected for the following systematic effects:

(i) Electronic and intrinsic gain. The gain of the electronics is measured using a calibration system which injects a pulse at the input to the preamplifier. A correction to this measured gain must be made to account for the resistors that couple neighboring channels. There are additional variations that are a function of the 72 sublayers due to small changes in the field shape. This effect is measured from the data and a correction applied for each sublayer.

(ii) Path length. A straightforward geometric correction is applied to account for the longer path length for angled tracks. In addition, the most probable energy loss has a logarithmic dependence on path length which is not directly corrected for. It is less than 2% for $|\cos\theta| < 0.6$. The resulting dependence on track angle θ is partially included in the saturation correction described below.

(iii) Temperature and pressure. The gas gain is a function of gas density and therefore sensitive to changes in temperature and pressure. In the Mark II chamber, thermistors and pressure transducers are used to monitor changes and the gain is corrected for each event. The thermistors (10 in all) are mounted outside the chamber in thermal contact with the cylindrical shell and the endplates. Gas pressure is measured by two transducers on each end which sample the gas through holes in the endplate. The relationship between gas gain g and gas density ρ was measured from the data to be approximately $\Delta g/g \simeq 6\Delta\rho/\rho$.

(iv) Wire Stagger. As can be seen in fig. 1, the sense wires are staggered $\pm 380\mu\text{m}$ from the cell axis to resolve the left-right ambiguity. Data shows that the average charge collected is about 20% lower if the ionization electrons from a track pass through the plane of potential wires ("far", wire staggered away from track) than if the electrons do not pass through the plane ("near", wire staggered towards track).

This difference has been confirmed by an electrostatic simulation of the drift cell and is due to asymmetries in electric field lines and collection optics for “near” and “far” sense wires.

(v) Drift Distance. The presence of electronegative gases (10% CO₂ plus any O₂ contamination) reduces the detected pulse height because of capture or attachment of the primary ionisation electrons as they drift towards the sense wire. This reduction depends upon drift time, but in the middle of the cell (where the drift velocity is constant) it is proportional to drift distance. In addition, the collected charge for tracks very close to the cell boundary or to the sense wire plane is very sensitive to drift distance because of electric field inhomogeneities in those regions. From data, a piece-wise linear fit is made of collected charge versus drift distance (see fig. 4) and using these fits, the collected charge is corrected to make it independent of drift distance.

(vi) Saturation. The arrival of the first electrons from primary ionization at the anode leaves behind a cloud of positive ions from the multiplication process. This cloud then reduces the amplification for later-arriving electrons. The result is that the charge deposited on the anode is no longer proportional to the primary ionization, an effect referred to as saturation. The effect decreases when the ionization is spread out along a length of the wire, as is the case for tracks angled away from $\theta = 90$ degrees and for large drift distances where diffusion spreads out the ionization. The result is a complicated dependence on track angle, drift distance, and primary ionization. Fig. 5 shows the saturation effect for several drift distances, measured with cosmic ray muons. A correction which fits the data reasonably well is of the form $(1 + A \sin \psi)/(1 + A)$ (solid curves in fig. 5) where $\psi = |\theta - \frac{\pi}{2}|$ and A is a function of the drift distance, d . A is parameterized in the form:

$$\ln A = c_1 + c_2 \times d \quad (3.1)$$

where the c_i are determined from fits to the data.

3.3. dE/dx DETERMINATION AND COMPARISONS TO MODEL

The most probable dE/dx is estimated by taking the mean of the smallest 75% of the corrected ionization samples. This truncated mean removes some of the fluctuations due to the large tail in the Landau distribution. A bias in the truncated mean method arises from the loss of samples due to the hardware threshold on pulse height. With fixed threshold, a minimum ionizing track loses more samples under threshold than a track with a higher mean ionization. To correct for this effect, tracks which show a TDC hit and no FADC hit (the TDC system has a much lower threshold) are treated as pulses just under threshold and added to the list of samples before taking the 75% truncated mean. In addition to discarding the large samples, the smallest 5% are also discarded to remove the added "fake" hits. Attempts are being made to lower the threshold and minimize this effect. Fig. 6 shows the resulting mean dE/dx versus momentum for cosmic ray muons. The solid curve is the prediction based on the standard formula [6,7] for the most probable energy loss, E (MeV), in a reduced thickness of gas, t (g/cm^2):

$$E = \frac{Z_{inc}^2 \alpha t}{\beta^2} \left[\ln \frac{m_e c^2 \alpha t}{I^2} + 0.891 + 2 \ln \beta \gamma - \ln \beta^2 - \beta^2 - \delta(\alpha t, \gamma) \right] \quad (3.2)$$

$$\alpha t = 0.1536(Z/A) \text{ (MeV for } t \text{ in } \text{g}/\text{cm}^2\text{)}$$

where Z_{inc} is the charge of the incident particle in units of electron charge, I is the mean ionization potential of the gas, Z and A are the charge and mass numbers of the gas, and δ is a density correction. The density correction used is a parametrization by Va'Vra [8] of experimental measurements of the relativistic rise in various gases [9]. The model of Allison and Cobb [10], which uses measured photoabsorption spectra to predict the most probable dE/dx , agrees with equation (3.2) within our experimental errors.

The residual disagreement in the relativistic rise in fig. 6 could be due to various systematic effects. In particular, the saturation effect will also cause a wire gain

suppression which depends on the primary ionization. This effect introduces a non-linearity which can reduce the relativistic rise. Because such an effect is difficult to remove from the data, for the purposes of particle identification the theoretical curve is shifted and scaled to bring it into agreement with the data.

Fig. 7 shows the measured dE/dx versus momentum for identified tracks with greater than 60 samples for data taken at PEP. Particles are identified either by other detector systems (e.g. protons identified by the time of flight system; muons from penetrating the iron of the muon system) or by topology (e.g. electrons from radiative bhabha events and pair conversions; pions from tau decays). Knowing the particle species, the theoretical curves are fitted to the data as outlined above and shown as the solid curves in fig. 7. The large cluster of tracks at a momentum of 14.5 GeV/c are the two-track Bhabha scattering events and muon pairs. The large number of proton tracks come predominantly from beam interactions with gas in the evacuated beampipe.

A dE/dx resolution of 6.9% is expected [8] for minimum-ionizing tracks with 72 charge measurements. The resolution for Bhabha electrons was determined by fitting a gaussian function to E , the measured most probable energy loss, to obtain $\sigma(E)/E = 7.0\%$. More recent cosmic ray data with the fully instrumented chamber give a resolution of 7.2%. The resolution dependence on number of samples agrees with other measurements [11] which find a $n^{-0.43}$ dependence.

3.4. PARTICLE SEPARATION PERFORMANCE

Using the measured resolution and the fit of the theoretical curve to the data one can predict the expected separation for various particle types. Fig. 8 shows the dE/dx separation, $\Delta E_{i/j} = E_i - E_j$, measured in number of standard deviations, σ , as a function of momentum for π/e , π/K and π/p combinations. These curves assume 72 samples per track, with ionization collected over a gas length of 8.33 mm.

Fig. 9 shows the separation between identified electrons and pions for the momentum range of 0.25 GeV/c to 0.60 GeV/c. The electrons are pair conversions or identified by the barrel electromagnetic calorimetry. The pions are identified from tau three-prong decays and tracks which are not identified as electrons, kaons, or protons. Muon contamination in the pion sample is estimated to be 0.1% .

4. Conclusions

Flash-ADC readout has been installed on the new central drift chamber for the Mark II detector at SLC. Systematic corrections to the most probable energy loss have been determined using a small sample of e^+e^- data taken at PEP and a cosmic ray sample. After applying the corrections, the resolution achieved is 7.0% for 14.5 GeV electrons. The dependence of energy loss on momentum has been measured and agrees well with a semi-empirical formula.

We would like to like to acknowledge the technical support of Dorel Bernstein, Joel Taylor, Jeff Olsen, Bob Bejsovec, Bob Gray, Mike Lateur, Tony Bell, Don Briggs, and Dave Wilkinson.

REFERENCES

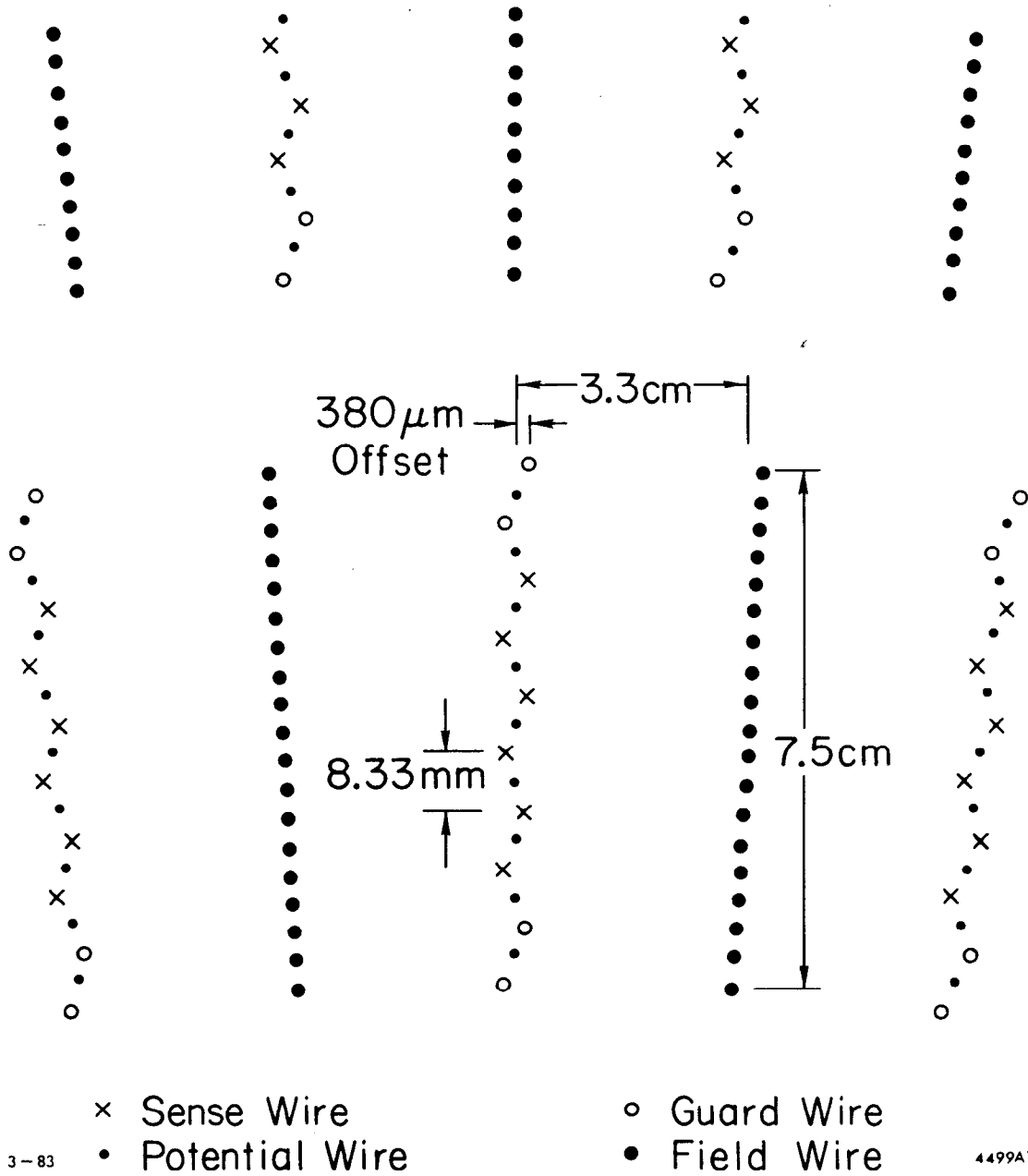
1. G. Hanson, *Nucl. Instr. and Meth.* **A252** (1986) 343.
2. D. Briggs, *et al.*, *IEEE Trans. Nucl. Sci.* **NS-32** (1985) 653.
3. D. Bernstein, *et al.*, *IEEE Trans. Nucl. Sci.* **NS-33 NS-33** (1986) 86.
4. H. Brafman, *et al.*, *IEEE Trans. Nucl. Sci.* **NS-32** (1985) 336.
5. D. Schaile, *Nucl. Instr. and Meth.* **A242** (1986) 247.
6. L. Landau, *J. Phys. USSR* **8** (44) 201.
7. R. Sternheimer, *et al.*, *Phys. Rev.* **B3** (1971) 3681.
8. J. Va'Vra, *et al.*, *Nucl. Instr. and Meth.* **A203** (1982) 109.

9. A. Walenta, BNL Report, BNL-28328 (1980).
10. W. W. M. Allison, *et al.*, *Ann. Rev. Nucl. Part. Sci.* **30** (1980) 253.
11. A. Walenta, *Nucl. Instr. and Meth.* **161** (1979) 45.

FIGURE CAPTIONS

- 1) Cell design for the Mark II central drift chamber.
- 2) Example of Flash-ADC output for two tracks crossing in a cell.
- 3) Efficiency for separating two tracks as a function of their distance apart for the central drift chamber FADCs (closed circle) and TDCs (X's).
- 4) Measured ionization versus drift distance for "near" (wire staggered towards track) and "far" (wire staggered away from track) samples. The solid lines are a piece-wise linear parameterization of the effect.
- 5) Gain suppression versus track angle due to saturation for various drift distances d .
- 6) Measured relativistic rise using cosmic ray muons compared to standard semi-empirical formula.
- 7) Most probable dE/dx versus momentum for e^+e^- data taken at PEP.
- 8) Particle separation measured in number of standard deviations, $\Delta E/\sigma$, as a function of momentum for π/e , π/K , and π/p combinations.
- 9) Electron-pion separation in the momentum range 0.25-0.60 GeV/c. The particles are from two different event samples and so are not in their usual proportions.

DRIFT CHAMBER WIRE PATTERN



3-83

4499A1

Fig. 1

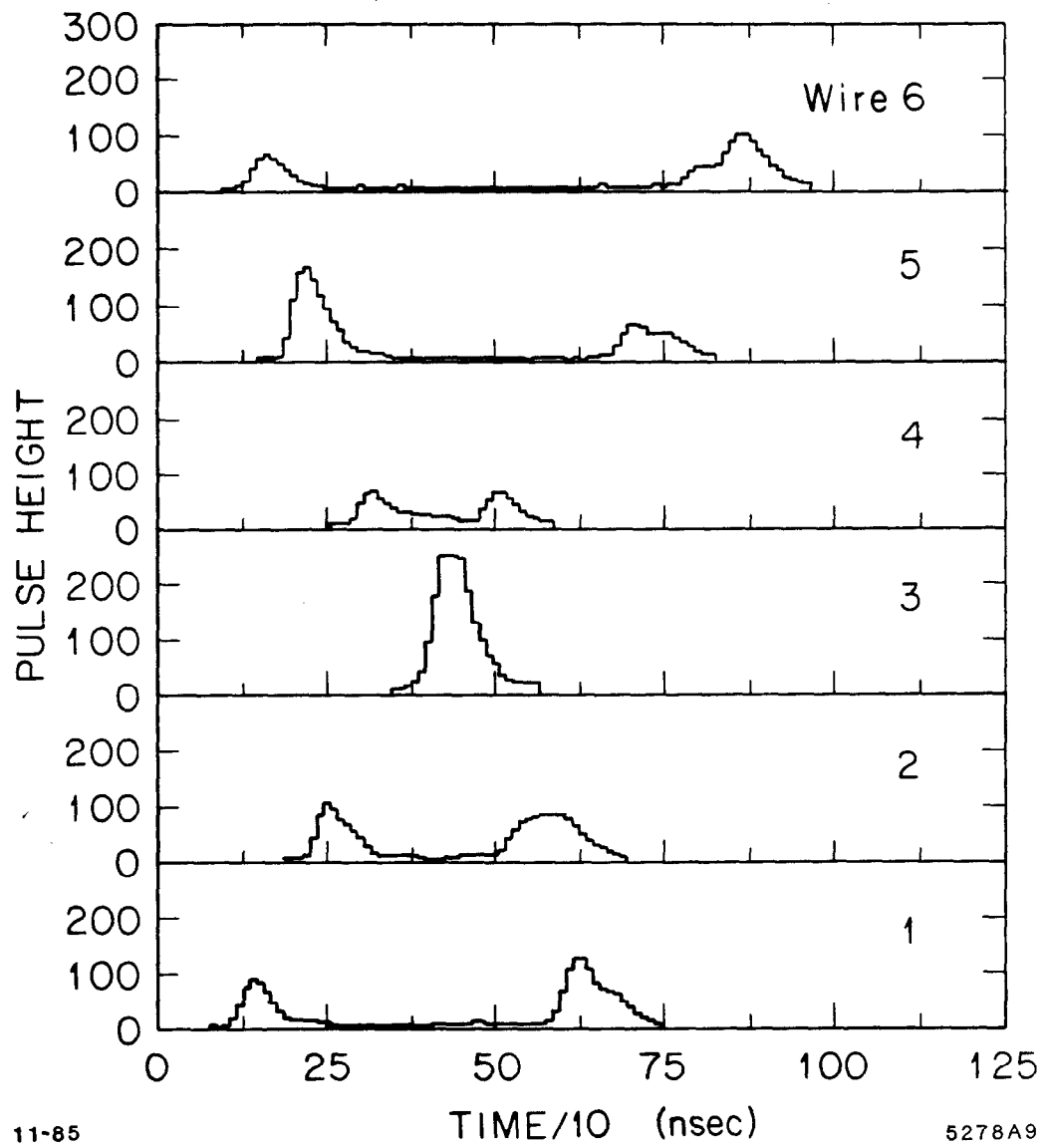
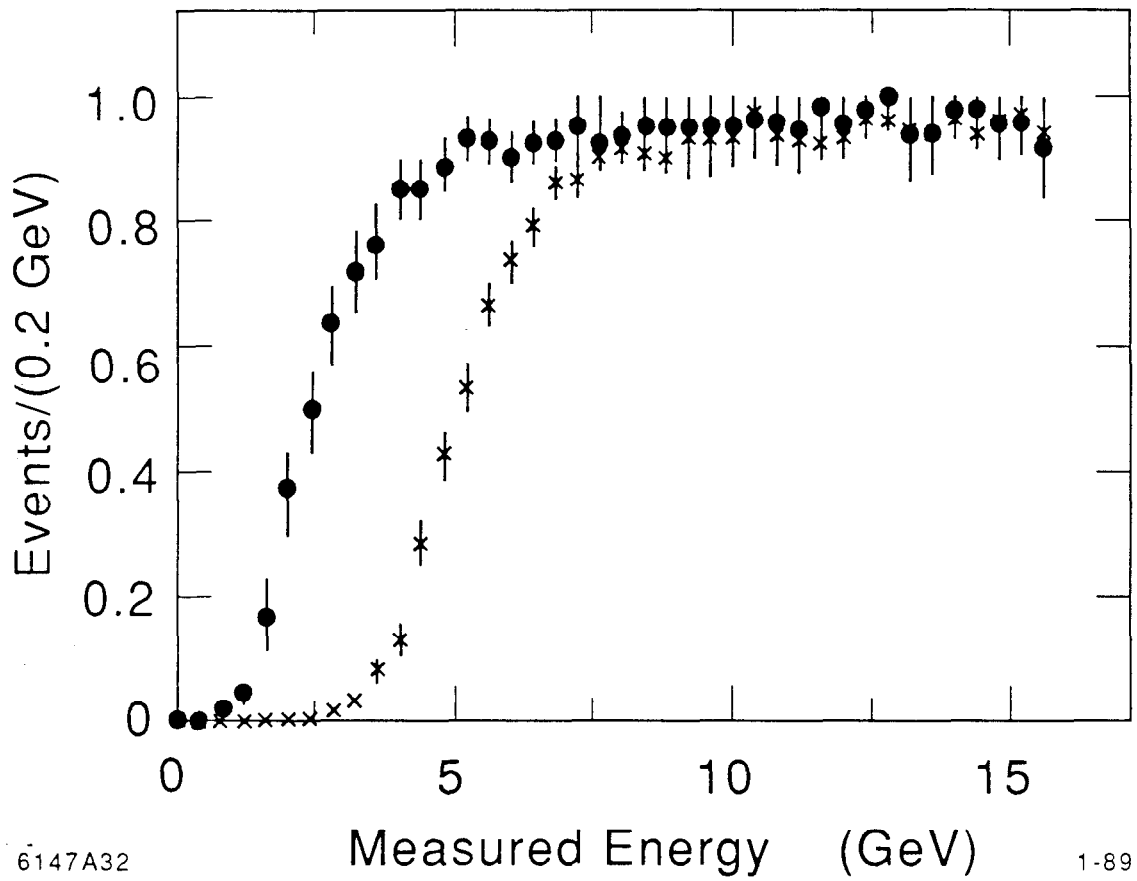


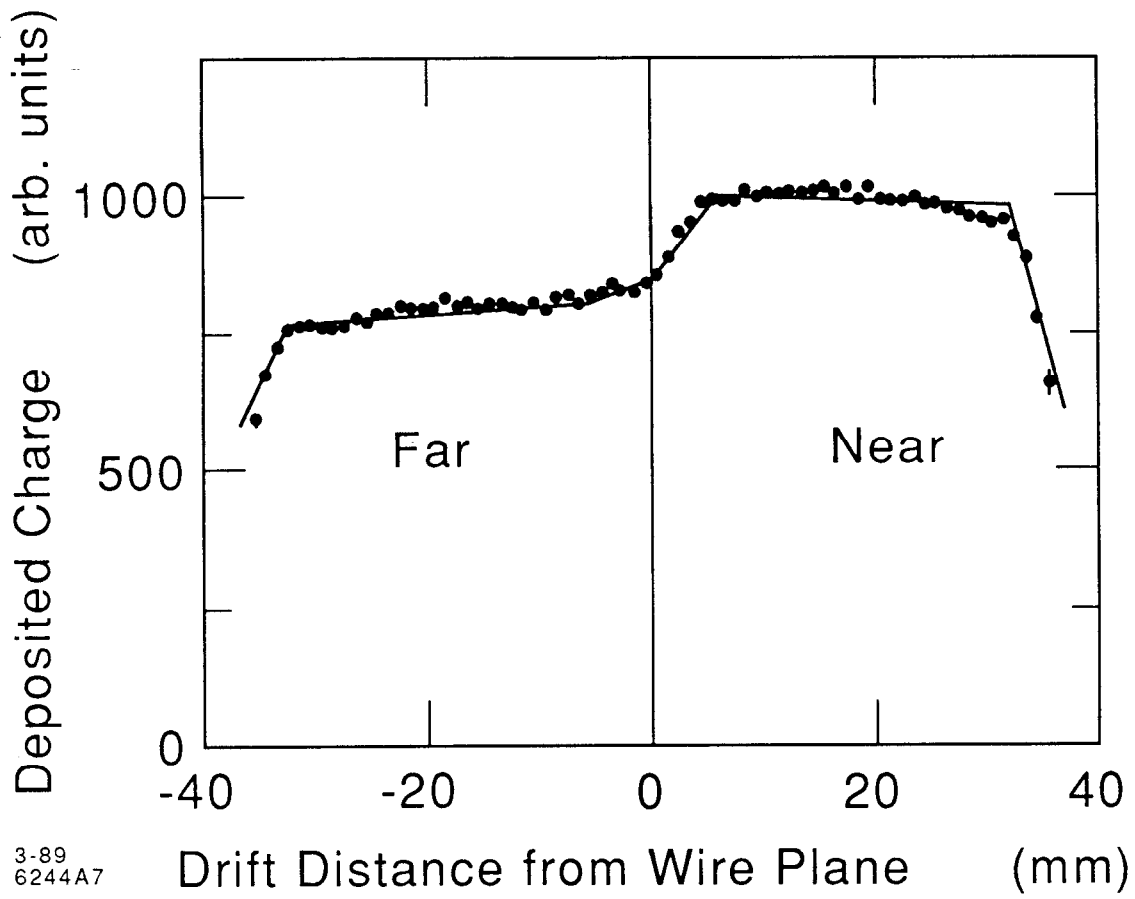
Fig. 2



6147A32

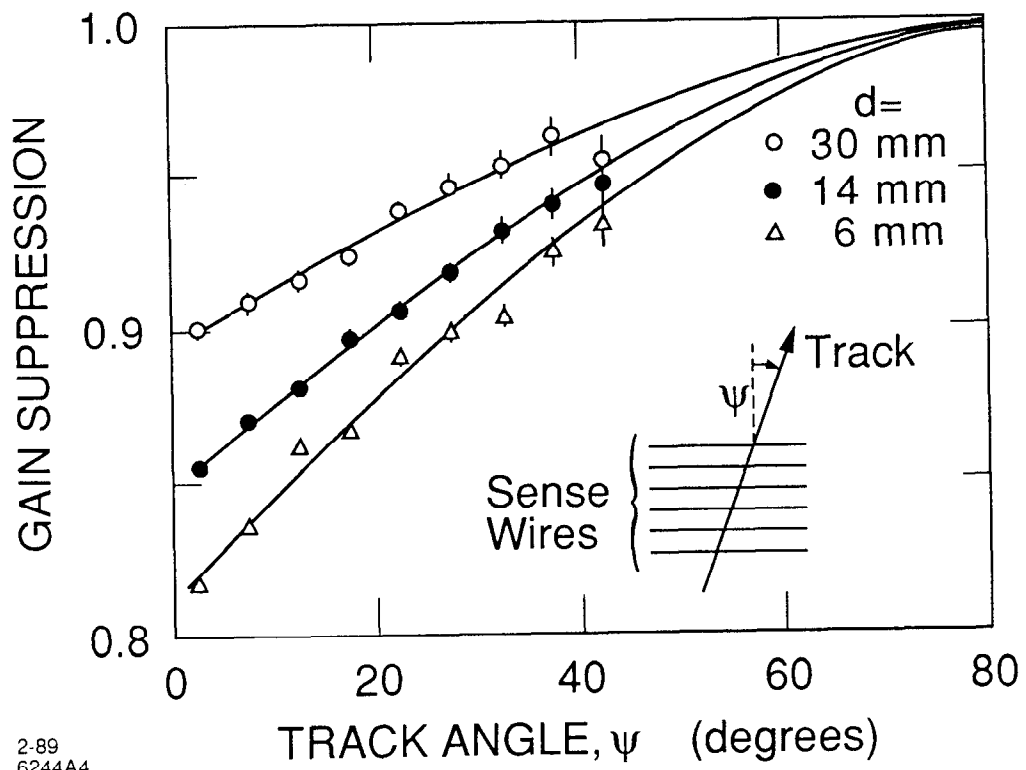
1-89

Fig. 3



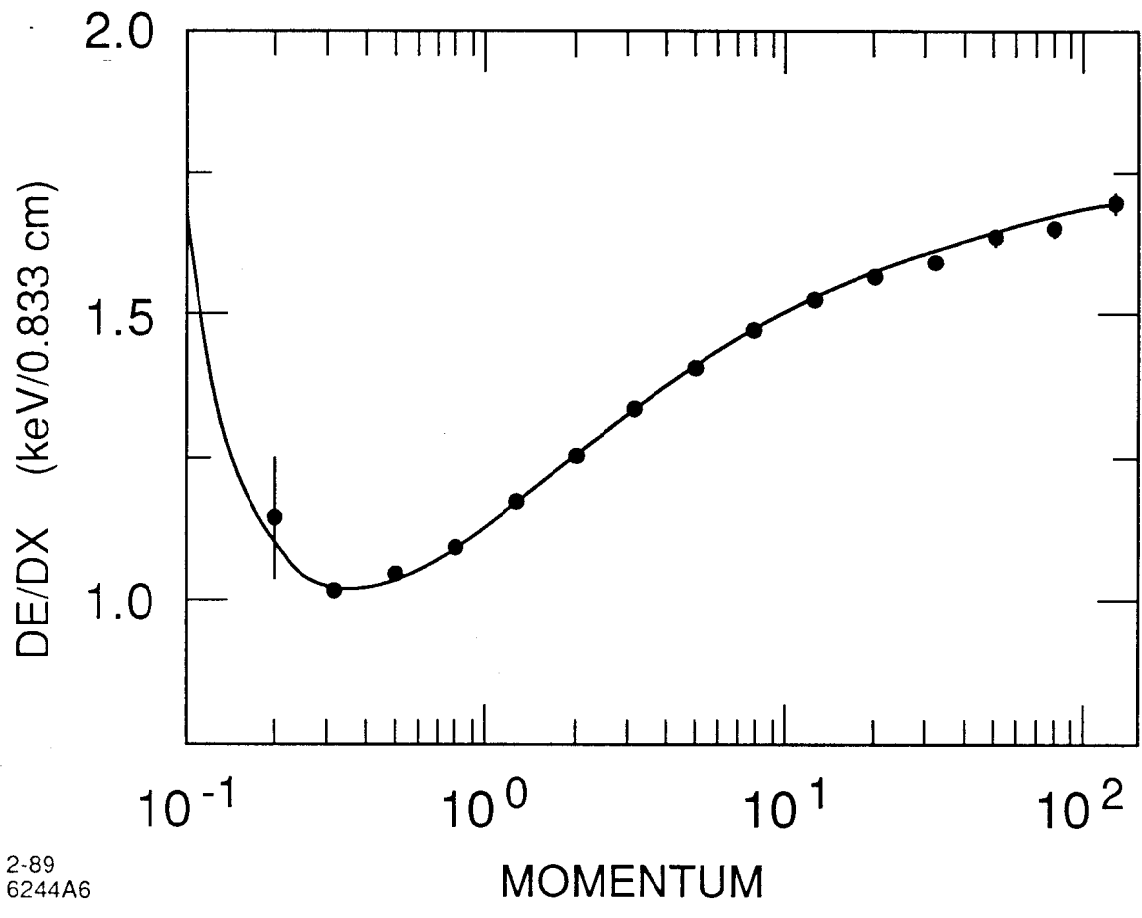
3-89
6244A7

Fig. 4



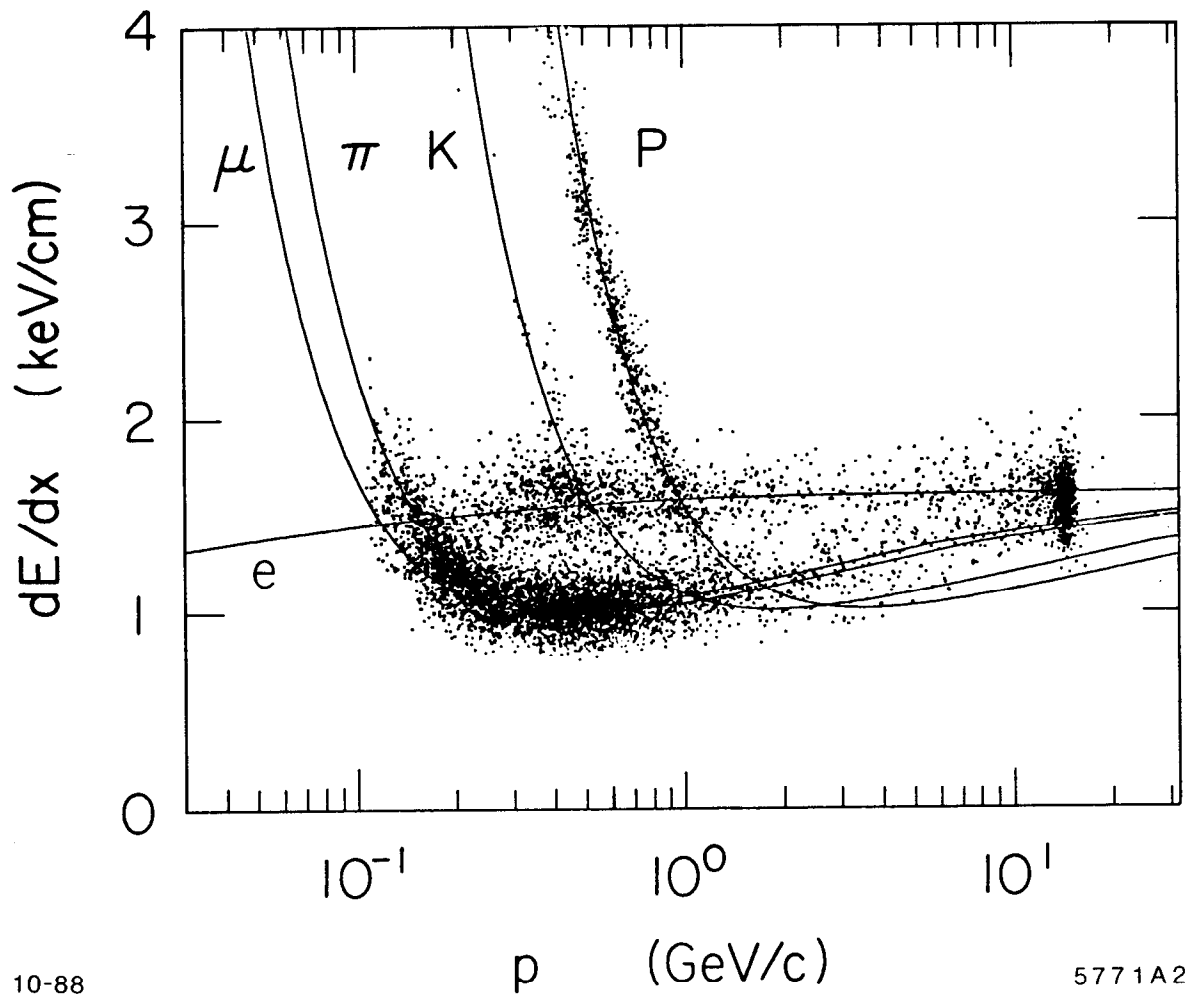
2-89
6244A4

Fig. 5



2-89
6244A6

Fig. 6

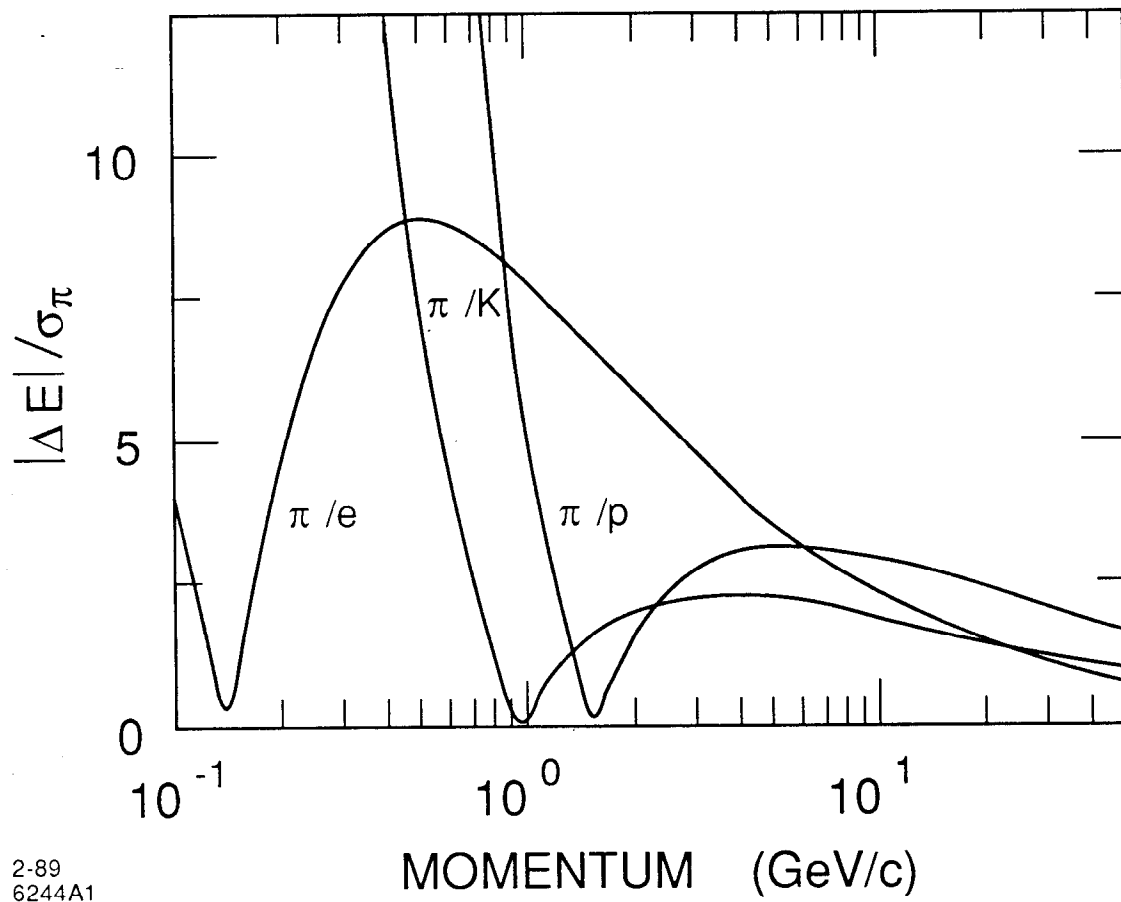


10-88

p (GeV/c)

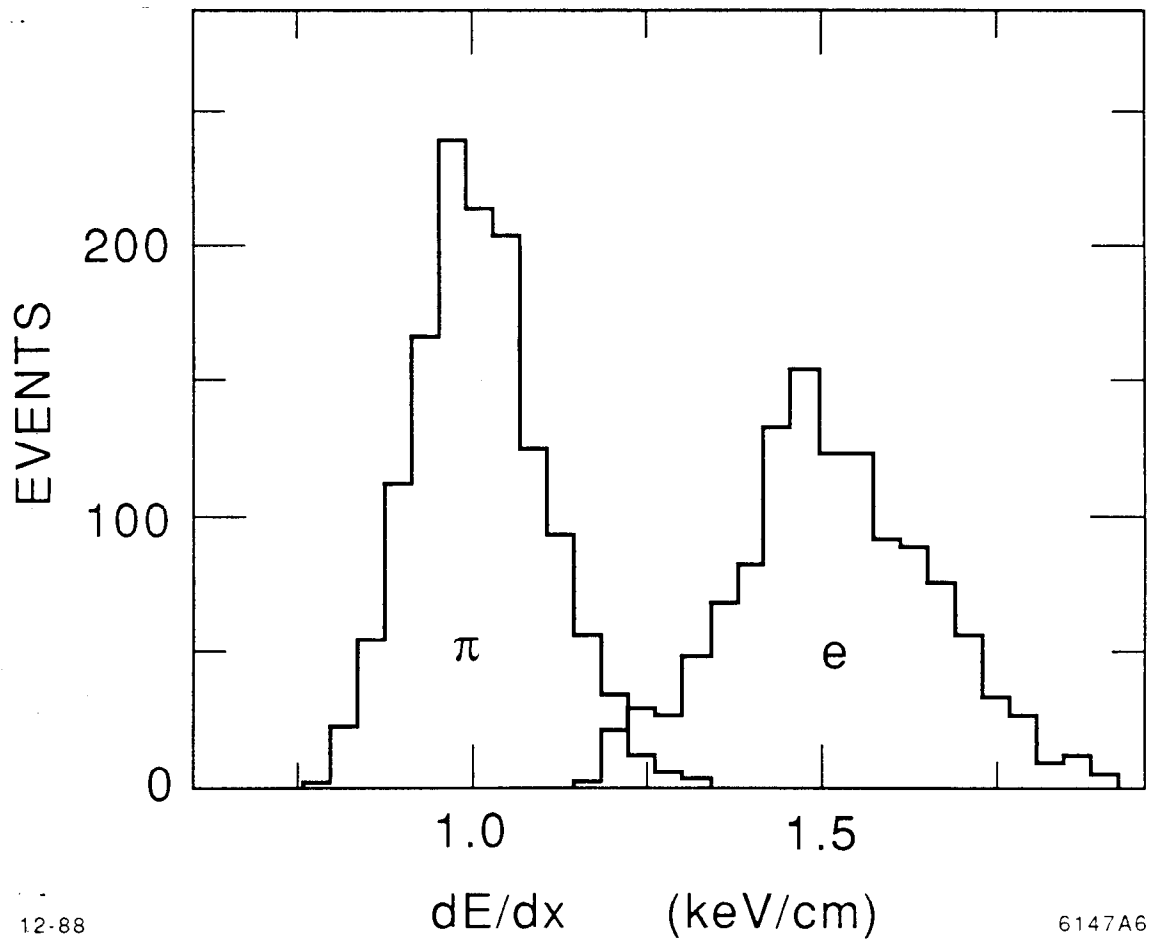
5771A2

Fig. 7



2-89
6244A1

Fig. 8



12-88

6147A6

Fig. 9